Phase transformations in epitaxial Ni/Fe bilayers upon low-temperature gaseous nitriding

A. V. Mijiritskii* and D. O. Boerma
Nuclear Solid State Physics, Materials Science Centre, University of Groningen, Nijenborgh 4, 9747 AG Groningen, The Netherlands
(Received 1 September 2000; revised manuscript received 28 March 2001; published 22 June 2001)

In this paper we describe studies on the low-temperature gaseous nitriding of epitaxial Ni-covered Fe layers. The epitaxial Ni/Fe bilayer system was grown by laser ablation deposition on an MgO(001) substrate. Nitriding was done in an NH_3+H_2 gas mixture in the 200 °C–300 °C temperature range. As a result of such nitriding, the main Fe-nitride phases could be produced as a pore-free material. The samples were analyzed by x-ray diffraction and conversion electron Mössbauer spectroscopy. It was observed that at the conditions applied the Fe-nitride phase formation occurs in the $\alpha\rightarrow\alpha'$, $\alpha''\rightarrow\gamma'\rightarrow\varepsilon\rightarrow\gamma'', \gamma'''$ sequence, whereby each step is accompanied by grain refinement. The precise orientation relationships between the phases in the $\alpha\rightarrow\alpha'$, $\alpha''\rightarrow\gamma'\rightarrow\varepsilon$ sequence were determined. Based on the data obtained, a model is proposed that describes this transformation sequence on an atomic scale in terms of martensitic transition. Among other results, evidence is provided for two different types of orientation relationships that can occur between α-Fe and γ'-Fe_4N, depending on the prevailing conditions. The morphology of the Ni/Fe-N system is discussed.

DOI: 10.1103/PhysRevB.64.035410 PACS number(s): 68.35.−p, 61.50.Ks, 64.60.My, 81.10.Aj

I. INTRODUCTION

For more than a century, nitriding has been used as a method to improve material properties of iron and steel. The Fe-nitride phases exhibit a variety of properties that are already employed, or can be of potential use, for numerous applications ranging from protective coatings to electromagnetic devices.

Atomic N can be dissolved in the body-centered-cubic (bcc) lattice of α-Fe to a concentration of about 0.4 at. % N without causing noticeable distortion of the bcc lattice. In the compositional range up to about 11 at. % N, the Fe-N compound is called nitrogen martensite α'. It has a body-centered-tetragonal (bct) lattice with the lattice parameters $a_{\alpha'}$ and $c_{\alpha'}$ in the 2.867–2.860 Å and 2.867–3.145 Å range, respectively, depending on the N content.[1] The N atoms occupy randomly octahedral hollow sites in the metallic sublattice. At saturation, nitrogen martensite has the Fe_8N composition. At this composition the α' phase can transform into the α'' phase. The α''-$Fe_{16}N_2$ phase differs from α'-Fe_8N by the distribution of the N atoms. In the α'' phase the N atoms are ordered.

In the γ-Fe phase, N can be dissolved to a maximum of 10.3 at. %. This phase has a face centered cubic (fcc) metal-atom arrangement with a lattice parameter in the range 3.572–3.652 Å depending the N content.[2] The γ'-Fe_4N phase has a narrow composition range of 19.3–20.0 at. % N. The Fe sublattice has the fcc structure with a lattice parameter $a_{\gamma'}=3.795$ Å . The N atoms occupy one quarter of the octahedral hollow sites in a fully ordered manner so as to minimize the strain energy and the mutual repulsion between N atoms.

The metal-atom arrangement in ε-Fe_xN is hexagonal close packed (hcp). The N atoms are randomly distributed in the octahedra formed by the Fe sublattice. The lattice parameters of this phase depend on the composition that can range from about 15 at. % N (at high temperatures) to 33 at. % N. At the Fe_2N stoichiometry, the ε phase of Fe nitride can be transformed into ζ-Fe_2N by ordering the N atoms over the octahedral sites so that an orthorhombic structure is formed.

Recently, the existence of two new cubic Fe-nitride phases has been reported.[3–5] One of them, γ''-FeN, has the ZnS-type of structure. The metal atoms form an fcc lattice with a lattice parameter $a_{\gamma''}=4.35$ Å. The other one, γ'''-FeN, is of the NaCl type with a lattice parameter $a_{\gamma'''}=4.52$ Å. In both phases N atoms are situated in tetrahedral hollow sites. Very little is known about these two phases and their properties.

A peculiar property of Fe-nitrides in relation with production and practical use is their metastability with respect to decomposition into N_2 and α-Fe (with a very low N content). This metastability makes it impossible to produce Fe nitrides by gaseous nitriding in N_2 gas. For instance, to form an ε nitride with 26 at. % N at 500 °C, a partial pressure of N_2 of the order of 10^5 atm is needed. For this reason, the production of Fe nitrides has been an issue for several decades and a number of nitriding methods has been developed.[6,7,4,8] The most commonly used process for Fe nitriding is by the action of NH_3 on the metal. The decomposition of the nitrides leads to the formation of N_2 bubbles in the interior of the Fe-nitride layer. These N_2-filled bubbles can coalesce to form pores. The rate-limiting step in the decomposition is the recombination of the N atoms into the N_2 molecules.[11,12] This recombination becomes significant only above 400 °C. Therefore, the formation of pores can be suppressed by applying lower temperatures during the nitriding process. However, the low-temperature regime has its own disadvantages, in particular, a low decomposition rate of NH_3 over the surface consisting of Fe or Fe nitride, and oxidation by trace amounts of H_2O or O_2 in the NH_3+H_2 gas mixture.[13] In addition, H_2O molecules adsorbed at the walls of the nitriding system are replaced by NH_3 molecules, so that the fraction of H_2O in the gas mixture is increased.

Recently, a method for low-temperature gaseous nitriding of Fe in an NH_3+H_2 mixture has been developed where a cap layer of Ni is used.[9,10] The role of Ni is twofold. On the one hand, it protects the underlying Fe from oxidation while

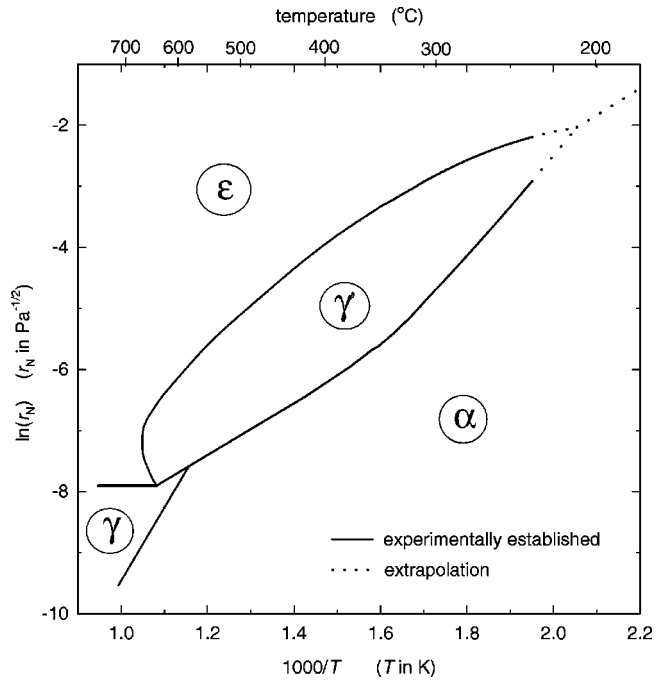

FIG. 1. The Lehrer diagram.

allowing transport of N. On the other hand, it serves as a catalyst promoting decomposition of NH_3. One of the advantages of this method is the ability to perform gaseous nitriding at relatively low temperatures resulting in the production of pore-free material.

The aim of the work described in this paper is to study the phase transformations taking place in thin epitaxial Fe films during low-temperature gaseous nitriding. For this purpose, a Ni cap layer is used during nitriding to produce the different Fe nitrides as a pore-free material. The orientation relationships (OR) occurring between the phases and the morphology of the samples produced are analyzed.

II. EXPERIMENTAL DETAILS

A MgO single crystal was cleaved in air along a (001) plane. Prior to the Ni/^{57}Fe deposition the substrate was annealed in vacuum (starting base pressure 5×10^{-10} mbar) at a temperature of about 600 °C for several hours to remove adsorbates and surface imperfections. The epitaxial Ni/^{57}Fe bilayers were grown on MgO(001) by laser ablation deposition. A yttrium aluminum garnet (YAG):Nd^{3+} laser ($\lambda = 1.06\ \mu$m) was used with an output energy of 250 mJ, operating in the *Q*-switched regime ($\tau = 15$ ns) with a repetition rate of 50 Hz. The material was ablated from ^{57}Fe and Ni targets mounted in an ultrahigh vacuum chamber, at a constant rate and constant energy distribution of the atoms in the laser plume. The deposition rate was monitored by an oscillating quartz crystal. The thicknesses of the ^{57}Fe and Ni layers were 100 nm and 25 nm, respectively. With x-ray photoelectron spectroscopy no Fe signal could be detected on Ni-covered Fe layers. This implies that the Ni forms a close layer. As has been reported earlier,[14] the overall OR in the epitaxial Ni/Fe/MgO(001) system is

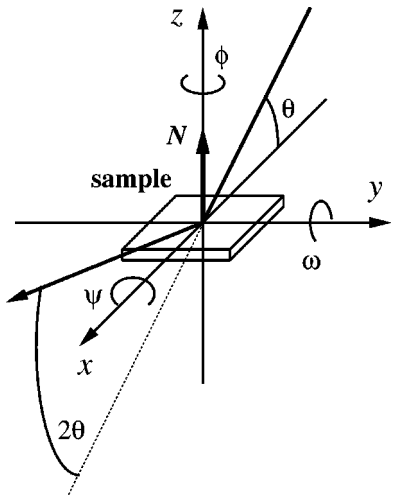

FIG. 2. Geometry of the XRD measurements. As-drawn, x rays incidence is in the *x*-*z* plane. θ-2θ scans are taken by rotating the sample (θ) and the detector (2θ) about the *y* axis. Azimuthal (ϕ) scans are taken by rotating the sample about the surface normal (**N**). Tilt (ψ and ω) scans are taken by tilting the sample about the *x* axis (ψ scan) and *y* axis (ω scan).

$$[110]_{\mathrm{Fe}}||[010]_{\mathrm{MgO}}, \tag{1}$$

$$(001)_{\mathrm{Fe}}||(001)_{\mathrm{MgO}}, \tag{2}$$

$$[1\bar{1}2]_{\mathrm{Ni}}||[110]_{\mathrm{Fe}}, \tag{3}$$

$$(110)_{\mathrm{Ni}}||(001)_{\mathrm{Fe}}. \tag{4}$$

After deposition the samples were transported to other systems for nitriding and further analysis.

Gaseous nitriding was performed in NH_3+H_2 gas mixtures in the 200 °C–300 °C temperature range. By applying low-temperature gaseous nitriding to the Ni/Fe system we succeeded in forming pore-free α''-, γ'-, ε, γ''-, and γ'''-Fe-nitrides. Which Fe nitride is formed at a given temperature depends on the nitriding potential, r_N. The so-called Lehrer diagram (see Fig. 1) gives boundaries in the r_N/T plane separating regions where a certain phase is formed in thermodynamic equilibrium.[15] The nitriding potential is given by $\ln(r_N)=p_{NH_3}/p_{H_2}^{3/2}$, where p_{NH_3} and p_{H_2} are the partial pressures of NH_3 and H_2 (in Pa) in the NH_3+H_2 mixture, respectively.[15,16,8]

In our experiments, characterization of the Fe-N phases was done by x-ray diffraction (XRD) and conversion electron Mössbauer spectroscopy (CEMS). XRD was also employed to determine OR's between the parent matrix and the phase formed. The XRD measurements were carried out in a Philips X'Pert-MRD system and in a conventional Philips XRD system using Cu $K\alpha$ radiation. Both offset and nonoffset geometries were utilized to analyze the sample structure. The geometry of the XRD measurements is explained in Fig. 2. In the CEMS measurements, the velocity of the radioactive source was calibrated by taking a spectrum on as-deposited Ni/^{57}Fe/MgO before the sample was subjected to any treatment.

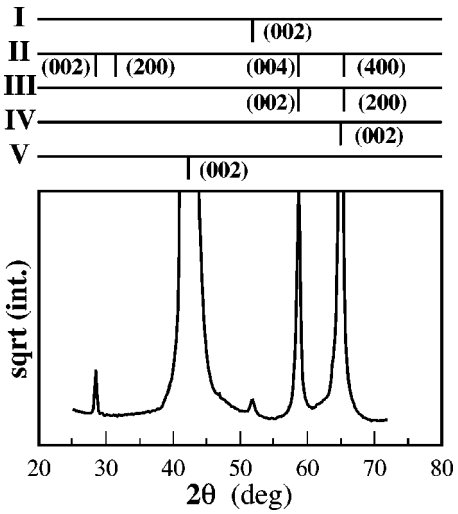

FIG. 3. A θ-2θ XRD scan recorded on a sample nitrided in pure NH_3 at 200 °C for 310 h. The bar diagram indicates the peak positions as observed for: (I) Ni, (II) α''-$Fe_{16}N_2$, (III) α'-Fe_8N, (IV) α-Fe, and (V) MgO.

III. RESULTS AND DISCUSSION

A. The α'-Fe_8N and α''-$Fe_{16}N_2$ phases

In Fig. 3 a θ-2θ XRD-scan is displayed that was recorded for a sample nitrided in pure NH_3 at 200 °C for about 310 h. Apart from the strong peak at about 42.9° due to the MgO(001) substrate and a small peak around 51.9° due to the Ni overlayer, all other peaks observed can formally be ascribed to a phase mixture of α-Fe and nitrogen martensite. The position and the width of the peaks due to martensite indicate that the nitride has a homogeneous composition close to Fe_8N. For α' phases with lower N content the peaks would be shifted to the higher 2θ values. The peak at 28.4° is the only feature in the scan that allows to distinguish between the α'-Fe_8N and α''-$Fe_{16}N_2$ phases. The peak is caused by ordering of N over octahedral sites in the α''-$Fe_{16}N_2$ phase, leading to a α''-$Fe_{16}N_2$ unit cell with dimensions twice that of α'-Fe_8N. Detailed analysis of the XRD peak positions showed that the c/a ratio of α'' in our sample is 1.097, which is slightly smaller than the value of 1.099 reported in the literature of a bulk α''-$Fe_{16}N_2$.[1,17] From x-ray scattering calculations, a value of 6.8 is expected for the intensity ratio between the (004) and (002) peaks of α''-$Fe_{16}N_2$.[18] In our experiments, this ratio was determined to be 12.7. This means that the XRD peak at 58.8° is constituted by both α''-$Fe_{16}N_2$(004) and α'-Fe_8N(002) reflections. Thus, the Fe nitride formed in the sample is a mixture of α'-Fe_8N and α''-$Fe_{16}N_2$ phases. It is interesting to mention here that the XRD spectrum reveals nitride peaks that are due to the $(00l)$ planes only. This means that the bct lattice of the nitride has its c-axis perpendicular to the sample surface. Our XRD measurements showed that

$$[001]_{\alpha',\alpha''} || [001]_{\alpha}, \tag{5}$$

$$(100)_{\alpha',\alpha''} || (100)_{\alpha} \tag{6}$$

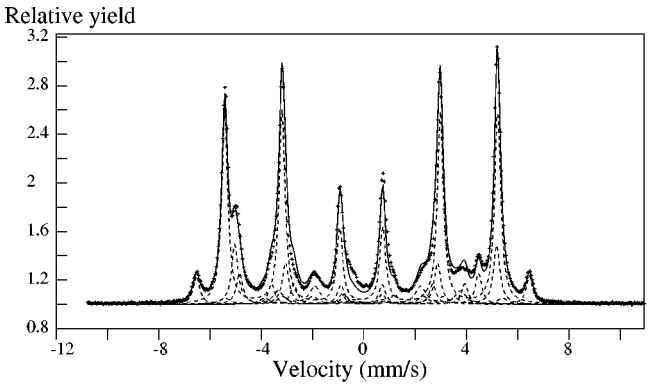

FIG. 4. A CEMS spectrum recorded on a sample nitrided in pure NH_3 at 200 °C for 310 h. See text for an explanation of the lines and symbols.

is the only OR present in the sample. This implies that during N uptake, expansion of the original bcc lattice occurs only in the direction perpendicular to the surface, as expected. Upon formation of α'-Fe_8N and α''-$Fe_{16}N_2$, the lattice parameters along the a and b crystallographic axes stay nearly unchanged while along the c axis the original bcc unit cell has to be expanded by approximately 10%. When the bct phase is growing, stress builds up in the crystal due to this distortion of the unit cell. In thin films, stress relaxation in the direction toward the surface is energetically favorable. In our samples this is the bcc-Fe[001] crystallographic direction that coincides with the surface normal. The formation of bct nitrogen martensite with a preferred c-axis orientation perpendicular to the surface has also been observed by de Wit and Saris, who studied Fe-nitride phase formation upon N implantation into Fe(001) single crystals.[19]

A CEMS spectrum obtained for this sample is shown in Fig. 4. In the figure, the symbols represent experimental data, the dashed lines represent different fit components, and the solid line is the total fit to the experimental curve. The $\alpha' + \alpha''$ phases together with α-Fe were found to constitute the major part of the spectrum (30.7% and 55.1%, respectively). Table I contains the hyperfine parameters found from the fitting procedure for the $\alpha' + \alpha''$ phase mixture. The fit could be improved by adding small components (14.2%) due to the γ' phase. The presence of a small fraction of γ'-Fe_4N in the sample was also proven by recording a θ-2θ XRD scan with an offset of 6° (not shown). The remaining misfit in the -0.7 mm/s to 1.3 mm/s part of the spectrum could be due to the presence of a very small (a few percent) fraction of nitrogen austenite (see Ref. 4 and references therein). Also,

TABLE I. Hyperfine parameters of the α''-$Fe_{16}N_2$ components obtained from the analysis of the CEMS data for the sample nitrided in pure NH_3 at 200 °C for 310 h.

Component	I.S. (mm/s)	H.F. (T)	Q.S. (mm/s)	Γ (mm/s)	Rel. area %
α''-Fe(I)	0.17(1)	40.27(8)	-0.20(2)	0.3	24.6
α''-Fe(II)	0.096(6)	31.67(4)	0.16(1)	0.3	49.7
α''-Fe(III)	0.00(1)	28.90(8)	-0.17(2)	0.3	25.7

we cannot exclude the formation of a tiny amount of $Fe_{1-x}O$ at the Ni/Fe interface. These fractions would be too small to be detected with XRD.

If we extrapolate the Lehrer diagram (see Fig. 1) to a temperature of 200 °C, the ε-Fe_xN phase should be formed in thermodynamic equilibrium at the nitriding conditions applied for this sample. However, no trace of ε-Fe_xN was found. Moreover, only part of α-Fe was converted into Fe nitride. This means that no thermodynamic equilibrium has been reached. Taking into account the diffusion coefficients reported in the literature,[20,21] diffusion of N cannot be a restriction for the phase formation at the temperature and nitriding time applied. At the same time, while a significant fraction of the α-Fe was still unaffected, the γ' phase had already started to form pointing to the fact that in the present experiment the kinetic barrier of transformation to this phase could be overcome. It was observed that the γ' and ε phases are readily formed when a bare epitaxial Fe(001) layer is exposed at 200 °C to a flow of atomic N.[22] The fact that we see only a small fraction of the γ' phase and no ε phase may be due to the slowness of the dissociation process at the surface, and/or the effectiveness of a kinetic barrier for the formation of the γ' and ε phases in the Ni-covered layer at the prevailing nitriding potential.

There have been a number of publications suggesting the existence of an α-γ'-ε triple point in the phase diagram.[23,24,8] Below the triple point no γ' can exist in thermodynamic equilibrium. The triple-point temperature reportedly lies well below 275 °C. Since in our experiment thermodynamic equilibrium has not been reached, no conclusions on the existence of the triple point can be drawn. However, if the temperature of the triple point lies above 200 °C, the appearance of γ' in our sample proves that in Fe the hcp ε phase must be formed from α-Fe via the fcc γ' phase.

B. The γ'-Fe_4N phase

In Fig. 5, θ-2θ XRD scans are displayed, which were acquired in nonoffset and offset geometries on a sample nitrided in a NH_3+H_2 mixture $[\ln(r_N)=-2.0]$ at 300 °C for about 10 h. Apparently, upon nitriding almost all α-Fe was converted into γ'-Fe_4N. This observation is in excellent agreement with the CEMS data as will be shown below. We have indications from Rutherford backscattering spectroscopy combined with channeling measurements (not shown) that the nucleation of the nitride phase takes place throughout the entire (100 nm) depth range of the Fe layer in the sample. This would be in accordance with the findings by Inia *et al.* for polycrystalline Fe samples covered with a Ni layer.[25]

From comparison of the two XRD scans it is obvious that the γ'-Fe_4N layer formed from a single crystal of α-Fe is heavily textured with its (001) planes slightly tilted with respect to the sample surface. To study the OR in greater detail, two-axes XRD scans were measured. Figure 6 displays an ω-2θ scan. During the scan the x-ray beam incidence was along the (010) plane of the MgO(001) substrate. The definition of the angles 2θ, ω, ψ, and ϕ is explained in Fig. 2. In

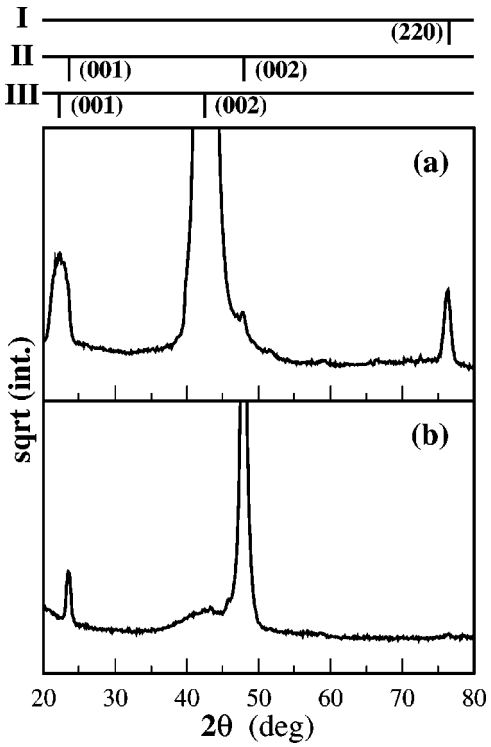

FIG. 5. A θ-2θ XRD scan recorded on a sample nitrided in a NH_3+H_2 mixture $[\ln(r_N)=-2.0]$ at 300 °C for 10 h: (a) with no offset; (b) with a 6° offset. The bar diagram indicates the peak positions as observed for: (I) Ni, (II) γ'-Fe_4N, (III) MgO.

Fig. 6, the two peaks observed at the 2θ values of 42.9° and 47.9° correspond to the MgO(002) and γ'-Fe_4N(002) reflections, respectively. Analysis of the peak positions along the ω scale showed that the offset between the (001) planes of γ'-Fe_4N and the (001) planes of the MgO substrate is 6.2°. The in-plane orientation of γ'-Fe_4N with respect to the substrate was derived by measuring ϕ-ω scans on the γ'-Fe_4N(113) and MgO(113) reflections (not shown). From the scans, the γ'-Fe_4N[010] || MgO[010] relationship was established. In Fig. 7, an ω-ψ scan is presented. In this measurement the 2θ angle was chosen to probe the γ'-Fe_4N(002) reflection and the x-ray beam was along

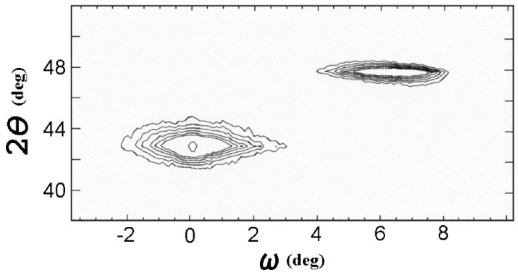

FIG. 6. An ω-2θ XRD scan recorded on a sample nitrided in a NH_3+H_2 mixture $[\ln(r_N)=-2.0]$ at 300 °C for 10 h. The intensity at $\omega=0°$ and $2\theta=42.9°$ is due to MgO(002); the intensity at $\omega=6.2°$ and $2\theta=47.9°$ is due to γ'-Fe_4N(002). The outer and inner MgO and γ'-Fe_4N intensity levels differ by a factor of 10^4 and 10, respectively.

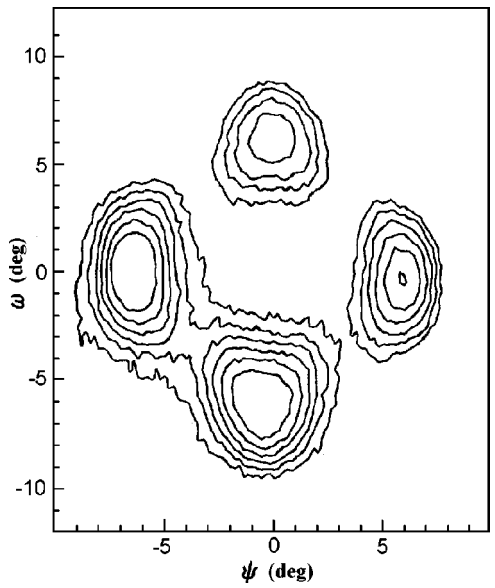

FIG. 7. An ω-ψ XRD scan of the γ'-Fe_4N(002) reflection recorded on a sample nitrided in a NH_3+H_2 mixture $[\ln(r_N)=-2.0]$ at 300 °C for 10 h. The first (outer) and the sixth contour lines differ in intensity by a factor of 3.

MgO(010) at $\psi = 0°$. The scan reveals four structural domains of γ'-Fe_4N with their (001) planes symmetrically tilted about γ'-Fe_4N[010] directions by 6.2° off the surface normal. Keeping in mind that Fe[110] || MgO[010] and Fe(001) || MgO(001), the OR between α-Fe and γ'-Fe_4N found in our experiments can be expressed as

$$[\bar{1}00]_{\gamma'}||[110]_{\alpha}, \tag{7}$$

$$(001)_{\gamma'}||(001)_{\alpha}R_{[110]}6.2°, \tag{8}$$

where $R_{[110]}6.2°$ denotes rotation by 6.2° around the $[110]_\alpha$ crystallographic direction.

A CEMS spectrum measured on this sample is shown in Fig. 8. In the figure, the symbols represent experimental data, the dashed lines represent different fit components, and the solid line is the total fit to the experimental curve. The spectrum could be fitted with sextets due to γ'-Fe_4N. We cannot

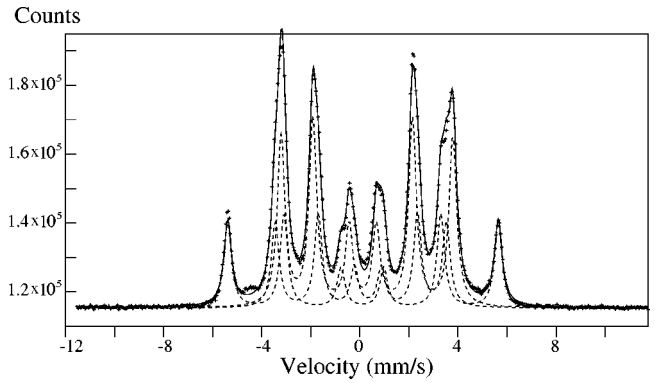

FIG. 8. A CEMS spectrum recorded on a sample nitrided in a NH_3+H_2 mixture $[\ln(r_N)=-2.0]$ at 300 °C for 10 h. See text for an explanation for the lines and symbols.

TABLE II. Hyperfine parameters obtained from the analysis of the CEMS data for the sample nitrided in a NH_3+H_2 mixture $[\ln(r_N)=-2.0]$ at 300°C for 10 h.

Component	I.S. (mm/s)	H.F. (T)	Q.S. (mm/s)	Γ (mm/s)	Rel. area %
γ'-Fe(I)	0.223(3)	34.18(2)	0.027(5)	0.380(3)	25.0
γ'-Fe(II)	0.311(1)	21.69(1)	0.175(3)	0.380(3)	50.0
γ'-Fe(III)	0.291(3)	21.62(2)	-0.291(6)	0.380(3)	25.0

exclude that there is a vary small (a few percent) fraction of the ε phase present in the sample, because there is a remaining misfit of the CEMS spectrum. This means that the nitride formed in the sample is almost a single γ' phase, which agrees well with our XRD observations. Since in γ' the Fe atoms are distributed over three different sites with a 1:2:1 occupation ratio, three sextets with the appropriate area ratios were used to fit the data. The line intensity ratio within each sextet was fitted to be $a:b:c$, with $a:c$ close to 3:1 and $a:b$ close to 3:3.5. The hyperfine parameters found from the fit are listed in Table II. The parameters are in good agreement with those reported in the literature (see Ref. 4 and references therein).

At the nitriding potential and temperature used in this experiment, the ε-Fe_xN phase should be formed according to the Lehrer diagram. In polycrystalline Fe samples covered with a Ni layer the formation of (nearly 100%) of the ε phase was observed at the conditions used here.[9,8] However, the nitride in our sample consists for more than 95% of the γ'-Fe_4N phase. The delay observed in the phase formation is probably due to a lack of nucleation sites (such as lattice defects or grain boundaries) in the epitaxial Fe layer, which causes high energy barriers for phase transitions. The importance of lattice defects during phase transformations has been proven by, e.g., Grujicic and Dang who carried out computer simulations on martensitic phase transformations in Fe-Ni alloys.[26]

C. The ε-Fe_xN phase

Two θ-2θ XRD scans recorded in nonoffset and offset geometries on a sample nitrided in a NH_3+H_2 mixture at $\ln(r_N)=0.0$ are shown in Fig. 9(a) and 9(b), respectively. The nitriding was done for 10 h at 300 °C. The set of peaks observed in the scans can be explained by the formation of the ε-Fe_xN phase in the sample. Apart from Fe nitride, the formation of Ni-nitride phases was also observed in the sample. Applying the formulas for the dependence of the lattice parameter on the N concentration c_N in ε-Fe_xN reported by Schaaf *et al.*,[4]

$$a_\varepsilon = 2.525 + 0.007\,47 \times c_N, \tag{9}$$

$$c_\varepsilon = 4.238 + 0.005\,65 \times c_N, \tag{10}$$

the composition as determined from our XRD data for the Fe nitride produced was $Fe_{2.17(2)}N$. Slightly different equations for the lattice parameter dependence were reported by Kooi.[27] However, in our studies we found that the equations

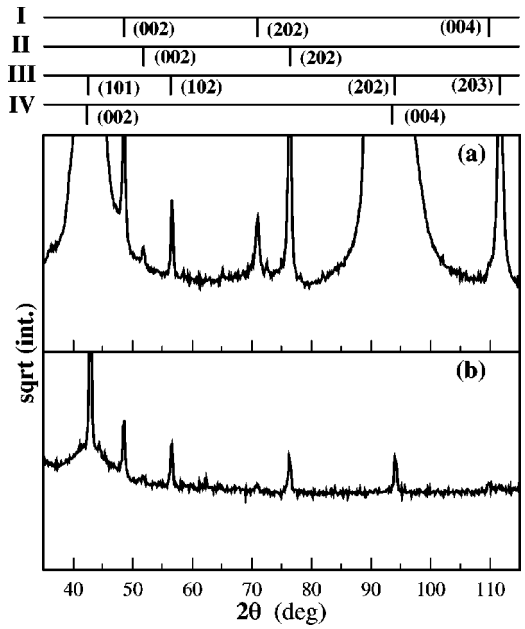

FIG. 9. θ-2θ XRD scans recorded on a sample nitrided in a NH_3+H_2 mixture $[\ln(r_N)=0.0]$ at 300 °C for 10 h: (a) with no offset; (b) with a 3° offset. The bar diagram indicates the peak positions as observed for: (I) Ni_4N, (II) Ni, (III) ε-Fe_xN, (IV) MgO.

due to Schaaf *et al.* give better agreement with our CEMS data. As can be seen from the XRD scans presented in Fig. 9, offsetting the sample results in a change in intensity ratios of the (102) and (203) reflections. This points to the presence of crystallographic texture in the Fe-nitride layer formed. It was determined that the (203) reflection reaches its maximum in the nonoffset case, meaning that the (203) planes of the nitride crystallites are parallel to the sample surface. Owing to the fourfold symmetry of the parent matrix, four different domains of the nitride can contribute to such a reflection. By analyzing with XRD the mutual orientation of the ε-$Fe_xN(101)$ and MgO(113) planes, the in-plane orientation of the ε-Fe_xN crystal with respect to the MgO(001) substrate was found to be ε-$Fe_xN[100]||$ MgO[110]. A two-axes ψ-ω scan measured for the ε-$Fe_xN(203)$ reflection is presented in Fig. 10. In this measurement, the x-ray beam was impinging on the sample along the MgO(110) plane at $\psi = 0°$. The scan reveals that the (203) planes are in fact slightly tilted with respect to the sample surface, giving rise to a crosslike shape of the peak. The tilt of the (203) planes is about 2°. Since the OR between α-Fe and MgO is Fe[110] || MgO[010] and Fe(001) || MgO(001), the overall OR between the ε-Fe_xN formed and the original α-Fe crystal is determined to be

$$[100]_\varepsilon||[0\bar{1}0]_\alpha R_{[0\bar{1}0]}2°, \tag{11}$$

$$(\bar{2}0\bar{3})_\varepsilon||(001)_\alpha R_{[0\bar{1}0]}2°. \tag{12}$$

It should be noted that it was not possible to determine the exact value of the tilt because of a strong overlap of the (203)

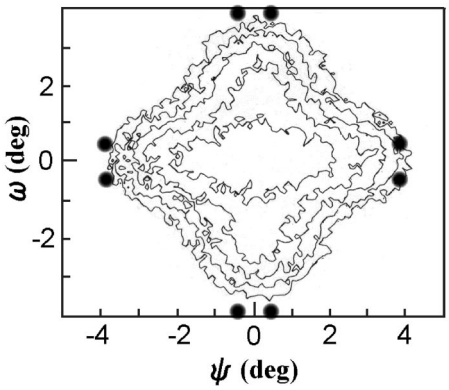

FIG. 10. An ω-ψ XRD scan of the ε-$Fe_xN(203)$ reflection recorded on a sample nitrided in a NH_3+H_2 mixture $[\ln(r_N)=0.0]$ at 300 °C for 10 h. The outer and inner contour lines differ in intensity by a factor of 4. The full circles indicate the positions of the maxima in the intensity predicted by our model.

reflections produced by twinned domains. From the analysis, a total of eight hcp ε-Fe_xN structural domains should be present in the sample.

A CEMS measurement revealed that for the nitriding conditions applied all Fe was converted into the ε-Fe_xN phase. The CEMS spectrum is presented in Fig. 11. From the shape of the spectrum it can be easily seen that at RT the major part of Fe nitride is nonmagnetic that holds for ε-Fe_xN phases with a N concentration above 30 at. %.[28] Our analysis showed that the CEMS spectrum consists of two quadrupole-split doublets plus a magnetically split component. The magnetic field experienced by the Fe atoms, causing magnetic splitting in the spectra, has a broad distribution up to *B* fields of about 29 T. To cover this range, in our analysis we fitted the magnetically split component with a broad sextet. The hyperfine parameters for the components, as obtained from the fit, are presented in Table III. The two quadrupole-split doublets [components Fe(II) and Fe(III) in Table III] point to the presence of two different Fe sites in the nonmagnetic phase. The areas of the doublets reflect the probabilities of the different Fe sites. On the basis of the nitrogen-ordering model proposed by Jack,[29] from the ratio between the doublet areas we obtained the composition as $Fe_{2.17(1)}N$ what is

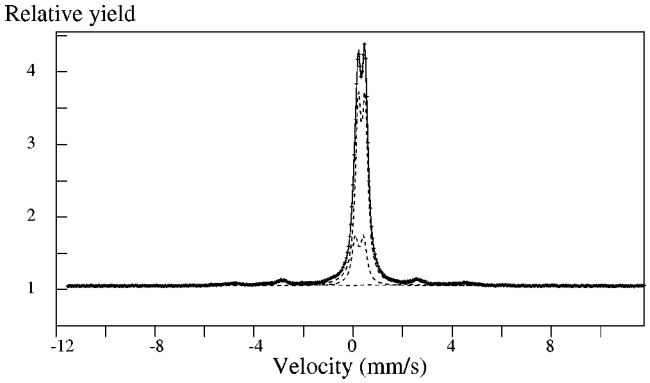

FIG. 11. A CEMS spectrum recorded on a sample nitrided in a NH_3+H_2 mixture $[\ln(r_N)=0.0]$ at 300 °C for 10 h.

TABLE III. Hyperfine parameters obtained from the analysis of the CEMS data for the sample nitrided in a NH_3+H_2 mixture $[\ln(r_N)=0.0]$ at 300 °C for 10 h. The notation for the different components is taken from Ref. 4

Component	I.S. (mm/s)	H.F. (T)	Q.S. (mm/s)	Γ (mm/s)	Rel. area %
ε-Fe(III)	0.453(0)		0.278(0)	0.280(1)	69.3(1)
ε-Fe(II)	0.360(2)		0.346(3)	0.311(4)	20.8(1)
M	-0.040(7)	29.215		0.72(2)	9.9(1)

in good agreement with our XRD data, if calculated in accordance with Eqs. (9) and (10). The hyperfine parameters of this phase are fairly close to those reported in the literature for an ε phase with the composition $Fe_{2.12}N$ by Schaaf *et al.*[4] and with the composition $Fe_{2.20}N$ by Chen *et al.*[28] The small (9.9%) total spectral area covered by the magnetically split sextet (component *M* in Table III) may be caused by ferromagnetic ε-Fe-nitride phases that have a Curie temperature above RT. The Curie temperature is a function of the N concentration. Fe_xN phases with $x \geqslant 2.2$ are ferromagnetic at RT.

A CEMS spectrum recorded on a sample nitrided in pure NH_3 at 300 °C for about 10 h is shown in Fig. 12. There are two major differences distinguishing this CEMS data from the one discussed above. First, no magnetic component is present. Second, a pronounced shoulder can be observed on the left-hand side of the quadrupole-split doublet. Fitting the spectrum with two quadrupole-split doublets resulted in a very broad smaller component with a large (nearly 1 mm/s) quadrupole splitting, pointing to the presence of more than two lines in the spectrum. The best fit was achieved with the hyperfine parameters presented in Table IV. The first two components correspond to the $Fe_{2.03(1)}N$ composition. On the basis of XRD data obtained for this sample, an $Fe_{2.03(2)}N$ composition was derived from Fe-nitride peak positions using Eqs. (9) and (10). The same OR between Fe nitride and the substrate was found as in the previous case. The remaining features in the CEMS spectrum (components B and D in Table IV) could be ascribed to a mixture of γ''-Fe_xN and γ'''-Fe_xN. The information on these two phases and, in particular, on their hyperfine parameters is very scarce. The hyperfine parameters found in our calculations for the γ''-Fe_xN + γ'''-Fe_xN mixture are in qualitative agreement with the values reported by Schaaf *et al.*[4] The deviation in the hyperfine parameters is most probably due to a variation in composition of the Fe_xN compounds with $1.0<x<1.6$.[30,3,31,4,32,5] Recent calculations, carried out on the basis of a first-principles method, showed that the magnetic moments in the Fe_xN phases with high N content are very sensitive to the Fe-N nearest-neighbor distance.[33] In our XRD measurements we did not find peaks corresponding to any of these two phases. The most plausible explanation would be that the fractions of the γ''-Fe_xN and γ'''-Fe_xN phases in the sample are too low to be detected with XRD, or that the crystallites of these phases are not oriented with planes parallel to the surface.

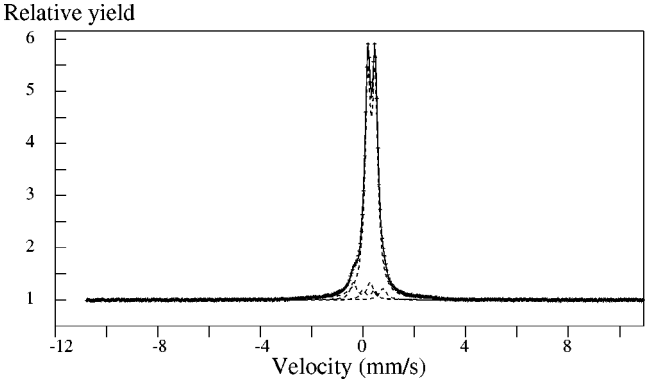

FIG. 12. A CEMS spectrum recorded on a sample nitrided in pure NH_3 at 300 °C for 10 h.

TABLE IV. Hyperfine parameters obtained from the analysis of the CEMS data for the sample nitrided in pure NH_3 at 300 °C for 10 h. The notation for the different components is taken from Ref. 4

Component	I.S. (mm/s)	H.F. (T)	Q.S. (mm/s)	Γ (mm/s)	Rel. area %
ε Fe(III)	0.437(1)		0.286(1)	0.264(2)	84.8(3)
ε Fe(II)	0.32(1)		0.450(0)	0.264(2)	3.5(4)
B	0.89(1)			0.34(0)	3.1(2)
D	0.060(6)		0.65(1)	0.30(0)	8.1(2)

D. Orientation relationships and morphology

Below we discuss a phase transformation model that can explain the OR's observed. Phase transformations in Fe-N (likewise in Fe-C) systems should be treated as of diffusional type since, in general, diffusion of both species occurs. However, in the temperature range (200 °C–300 °C) addressed in this work diffusion of Fe atoms is negligible.[34,35] Therefore, transformations in our samples can be regarded as diffusionless, as far as the Fe sublattice is concerned. We will show that, during low-temperature gaseous nitriding of α-Fe, phase transformations can be well described in terms of martensitic transitions. A martensitic transition is characterized by a synchronized movement of the lattice atoms by a distance less than one interatomic spacing. In a martensitic transition a habit plane exists, which has the same orientation before and after the transition and stays practically undistorted upon the transition.[36,37] It should be noted that we are dealing with thin epitaxial films. For bulk polycrystalline materials the transformations may deviate from those presented here.

In our consideration we assume that during gaseous nitriding the concentration of N in the sample increases gradually. During this gradual increase different phases can be formed in sequence according to the Fe-N phase diagram.[38,1] The final concentration of N is determined by the temperature combined with the nitriding potential applied. Since in the temperature range used in our experiments any of the α'-, α''-, γ'-, ε-Fe-nitride phases could be formed by gaseous nitriding, it would be plausible to assume that the phase transformations taking place in the sample occur in the α

$\rightarrow\alpha'$, $\alpha''\rightarrow\gamma'\rightarrow\varepsilon$ sequence. In terms of crystallography this route can be expressed as a bcc→bct→fcc→hcp phase transition.

During early N uptake, bct nitrogen martensite is formed. Although the occupation of the octahedral interstices causes large anisotropic strains in the Fe matrix, the bct lattice of martensite has about the same dimensions along two of its principal axes as those of α-Fe. Therefore, the basic OR between the martensite and the original α-Fe should not be affected by the transformation. With this in mind, the OR observed in the experiments [see Eqs. (5) and (6)] can be readily understood. The bcc→bct transition leading to such an OR is the most energetically favorable since no interatomic bonds are broken during the transformation process and thus the energetic barriers of the phase transformation are only determined by elastic distortion of the lattice. In the particular case of thin films the strain is relaxed to the surface.

Further N uptake leads to a bct→fcc transition. The critical point at which the transition takes place is associated with the point where strain relief by shear and sliding becomes energetically more favorable than by further elastic distortion of the lattice.

For the Fe-N system two essentially different OR's connecting bcc, bct, and fcc phases have been reported in the literature. The one commonly observed upon reducing the γ'-Fe_4N phase to α-Fe in thick (about 0.1 mm) films and in bulk material[39,40] is

$$[110]_{\gamma'}||[0\bar{1}0]_{\alpha}, \tag{13}$$

$$(\bar{1}12)_{\gamma'}||(201)_{\alpha}. \tag{14}$$

A theoretical analysis of the transformation leading to this OR has been carried out by Pitsch.[41] The OR was thought to be the result of the following three processes: (i) Bain deformation leading to an fct structure; (ii) shear in the $(111)_{\mathrm{fct}}$ plane along the $[11\bar{2}]_{\mathrm{fct}}$ direction of the newly formed fct; (iii) two small rigid rotations of the fct giving rise to an fcc structure. The other OR, namely,

$$[0\bar{1}1]_{\gamma}||[\bar{1}11]_{\alpha'}, \tag{15}$$

$$(011)_{\gamma}||(1\bar{1}2)_{\alpha'} \tag{16}$$

has been reported in only one instance[42] and no other experimental data has been published. Produced upon quenching of thin (100 Å) films of nitrogen austenite, this OR is formed by a combination of a distortion along the principal axes of austinite and a half twin shear in the $(110)_{\mathrm{fcc}}$ plane along the $[1\bar{1}0]_{\mathrm{fcc}}$ direction. In the course of the discussion we will refer to these two OR's as of *type I* OR and *type II* OR, respectively. These two OR's are different from the Kurdjumov-Sachs and Nishiyama-Wassermann types of OR observed in Fe-C and Fe-Ni systems.[43,44]

Comparing the above OR's with the results of our experiments, it can be seen that the relationship (15) follows from the OR found in our measurements [see Eqs. (7) and (8)] and

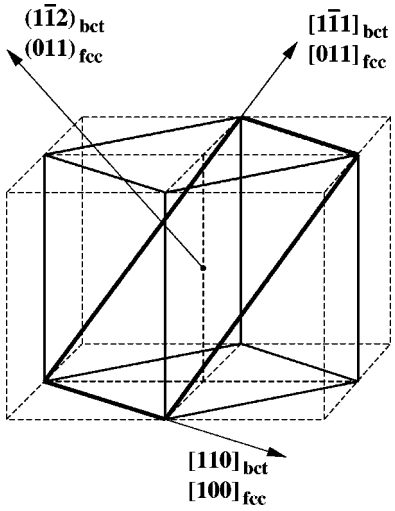

FIG. 13. An illustration of how the *type II* OR between a bct and an fcc structure can be accomplished by a Bain deformation alone. Four bct unit cells with a $(c/a)_{\mathrm{bct}}$ ratio of $\sqrt{2}$ are represented by dashed lines. Solid lines outline an fcc unit cell.

is not fulfilled in the *type I* OR. On the basis of this observation, the occurrence of the *type I* OR in our samples can be excluded.

The atomic movements associated with the *type II* OR are illustrated in Figs. 13 and 14 for our case. As can be seen from Fig. 13, the *type II* OR between bct and fcc lattices can in principle be achieved by a Bain deformation only. However, it would require a very big elastic distortion of the bct lattice, with a c/a ratio of $\sqrt{2}$. Such a big distortion probably cannot be realized for the $\alpha',\alpha''\rightarrow\gamma'$ transition and the transformation proceeds by a different mechanism. This assumption is supported by the existence of a finite tilt angle between the $(001)_{\mathrm{bct}}$ and $(001)_{\mathrm{fcc}}$ planes, which would not

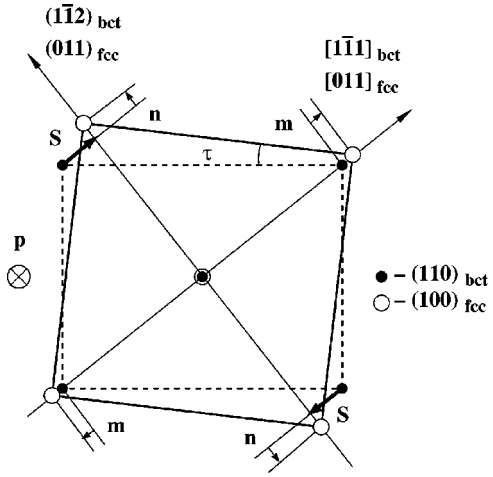

FIG. 14. An illustration of how a $(110)_{\mathrm{bct}}$ plane could possibly transform into a $(100)_{\mathrm{fcc}}$ plane. The transformation consists of (i) half twin shear (vector **S**) in the $(1\bar{1}2)_{\mathrm{bct}}$ plane along the $[1\bar{1}1]_{\mathrm{bct}}$ direction; (ii) small shifts (vectors **m** and **n**) to obtain the correct γ' lattice parameters within the $(100)_{\gamma'}$ plane; (iii) a small shift (vector **p**) of all atoms in the plane to obtain the correct spacing between the $(100)_{\gamma'}$ planes.

arise otherwise. We suggest that the following processes are most likely to take place upon the transition. Once a certain ''critical'' c/a ratio of the bct phase has been reached, deformation by an elastic distortion only is no longer favorable and the fcc γ' phase is formed by a half twin shear in the $(1\bar{1}2)_{\mathrm{bct}}$ plane along the $[1\bar{1}1]_{\mathrm{bct}}$ direction (vector **S** in Fig. 14). In this case, only small additional atomic shifts would be needed to obtain the correct lattice parameter of the fcc γ' phase within the $(001)_{\mathrm{fcc}}$ plane (vectors **m** and **n** in Fig. 14). As can be seen from the figure, the vector sum of **m** and **n** leads to a small expansion of the lattice, which is in the direction of the c axis of the α' phase, i.e., in the direction of the surface, and a small contraction in the surface plane along the $[1\bar{1}0]_{\mathrm{bct}}$ direction. Finally, a contraction along $[110]_{\mathrm{bct}}$ (vector **p**) is also necessary to adjust the distances between the $(001)_{\mathrm{fcc}}$ planes. The $(1\bar{1}2)_{\mathrm{bct}}$ and $(011)_{\mathrm{fcc}}$ planes stay parallel during this transformation because the displacements **S**, **m**, and **p** are in this (common) planes, whereas **n** is normal to these planes and, if measured from one $(1\bar{1}2)_{\mathrm{bct}}$ plane, the displacements **n** are equal.

In our experiments the tilt angle, denoted by τ in Fig. 14, was determined to be 6.2°. Such a tilt implies that the shear process started at a ''critical'' $(c/a)_{\mathrm{bct}}$ ratio of 1.137. This ratio is only slightly larger than that of bulk α'' and significantly smaller than the value needed if the bct→fcc transition would occur by a Bain mechanism alone. In fact, the c/a ratio at which the shear begins–and consequently the final tilt angle–can depend on the crystalline quality and the morphology of the sample. For our experimental conditions, the relatively large c/a ratio can be explained as follows. We have already mentioned above that a significant delay in phase formation has been observed in our experiments and a higher nitriding potential had to be applied to produce a certain Fe-nitride phase. This phenomenon has been attributed to the lack of nucleation sites in the epitaxial layers used as compared with polycrystalline material. The delay implies that larger lattice strain may be needed to make the transition happen. In the case of the bcc→bct→fcc transition described here, larger strain would result in a bigger anisotropic distortion of the lattice and, therefore, a larger c/a ratio in the bct phase. The influence of strain on the c/a ratio in nitrogen martensite has also been observed by Okamoto *et al.*[18]

The last question left to be discussed in conjunction with the $\alpha \rightarrow \gamma'$ transformation in the Fe-N system is the occurrence of different OR's. It is interesting to note in this respect that *type I* OR and *type II* OR have, in fact, been reported for two different cases as follows. The *type I* OR is observed as a relationship between the fcc lattice of γ' and the bcc lattice of α-Fe.[45,46,40] This OR seems to be realized when γ' is formed directly from α-Fe. Studies by Inokuti *et al.*,[45] e.g., give evidence that different Fe-nitride phases, and the γ' phase in particular, can form directly from α-Fe at the surface of Fe crystallites exposed to NH_3+H_2 mixtures in the 450 °C–550 °C temperature range. In this case, the γ' phase was found to nucleate with the *type I* OR. In contrast, the *type II* OR is observed as a relationship between the fcc lattice of γ' (or γ) and the bct lattice of α'/α'' (see Ref. 41 and this work). As a hypothesis we propose that the *type I* OR applies when the γ' phase is formed directly from bcc α-Fe and the *type II* OR applies when the fcc phase is formed via the bct α'/α'' phases.

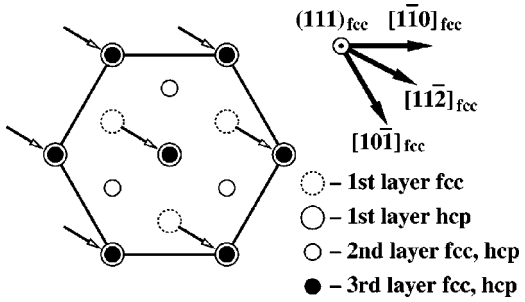

FIG. 15. An illustration of how a $(111)_{\mathrm{fcc}}$ could possibly transform into $(001)_{\mathrm{hcp}}$ by half twin shear in the $(111)_{\mathrm{fcc}}$ plane along the $[11\bar{2}]_{\mathrm{fcc}}$ direction.

Summarizing, the $\alpha \rightarrow \gamma'$ transformation in thin epitaxial Fe films at temperatures in the 200 °C–300 °C range can be well described in terms of a martensitic transformation of the Fe-sublattice. The transformation proceeds via a bct phase, it leads to an OR that is expressed as

$$[0\bar{1}1]_{\gamma'} || [\bar{1}11]_{\alpha'}, \tag{17}$$

$$(011)_{\gamma'} || (1\bar{1}2)_{\alpha'} \tag{18}$$

and features parallelity of close-packed directions (c.p.d.'s) between the precipitates and the parent matrix.

Now let us consider the α/ε system. Since phase transformation in Fe nitrides is driven by N diffusion resulting in a gradual change of N concentration in the sample, at the temperatures applied in our experiments one could expect that γ' is formed as an intermediate phase during the $\alpha \rightarrow \varepsilon$. Hence, it is the bcc-$\alpha \rightarrow$ fcc-$\gamma' \rightarrow$ hcp-ε transition that should be considered. The first part of the transition has been discussed above. Now we concentrate on the $\gamma' \rightarrow \varepsilon$ transition.

If no significant diffusion of the lattice atoms takes place, the

$$[010]_{\mathrm{hcp}} || [1\bar{1}0]_{\mathrm{fcc}}, \tag{19}$$

$$(001)_{\mathrm{hcp}} || (111)_{\mathrm{fcc}} \tag{20}$$

OR is the one observed in virtually all hcp/fcc systems.[47] This is due to the high degree of coherence between c.p.d.'s and close-packed planes (c.p.p.'s) of the two lattices. For the ideal case, perfect coherence occurs if $a_{\mathrm{hcp}} = a_{\mathrm{fcc}}/\sqrt{2}$ and $(c/a)_{\mathrm{hcp}} = 2\sqrt{\frac{2}{3}}$. The transformation occurs by shear of every other $(111)_{\mathrm{fcc}}$ plane along the $[11\bar{2}]_{\mathrm{fcc}}$ direction as shown in Fig. 15. Since the lattice parameter relations of ε-Fe_xN and γ'-Fe_4N deviate from the above values just slightly, the coherence can be achieved by shear plus a small distortion of the γ'-Fe_4N lattice.

In the hcp lattice of ε-Fe_xN, the angle between $(\bar{2}0\bar{3})_{\varepsilon}$ and $(001)_{\varepsilon}$ planes is about 51.3°. This angle can vary by a few tenths of a degree depending on the N content. The

angle between $(001)_{\gamma'}$ and $(111)_{\gamma'}$ planes in γ'-Fe_4N is 54.7°. On the one hand, if the relationships defined by Eqs. (19) and (20) are fulfilled, then we have $(\bar{2}0\bar{3})_\varepsilon || (001)_{\gamma'} R_{[1\bar{1}0]} 3.4°$, where $R_{[1\bar{1}0]}$ implies tilt around $[1\bar{1}0]$ of γ'-Fe_4N. On the other hand, as has been shown above, the lattice of γ'-Fe_4N is tilted with respect to the parent α-Fe crystal around Fe[110]. Considering four γ'-Fe_4N domains, a combination of the two different tilts will give rise to the ω-ψ diffraction peak positions for the ε-$Fe_xN(\bar{2}0\bar{3})_\varepsilon$ reflection as depicted by full circles in Fig. 10. In the figure, the diffraction peak positions of the double-tilted $(\bar{2}0\bar{3})_\varepsilon$ planes are indicated with full circles. As can be seen, four doublets are expected. The angle between $(\omega;\psi) = (0;0)$ and a doublet is 3.9°. In our measured scan (see Fig. 10), the doublets overlap and the peaks within a doublet are not distinguished. This is probably due to a finite width of the peaks. From a deconvolution procedure the angle between $(\omega;\psi) = (0;0)$ and a doublet was estimated to be $2 \pm 1°$. Within the error bar, this value deviates from the value calculated on the basis of 3.4° and 6.2° tilts by 1°.

According to Inokuti *et al.*,[45] exposure of α-Fe crystallites to $NH_3 + H_2$ mixtures in the 450 °C–550 °C temperature range results in the ε phase formation directly from α-Fe with the OR

$$[100]_\varepsilon || [2\bar{1}\bar{1}]_\alpha,$$

$$(001)_\varepsilon || (111)_\alpha.$$

In their experiments, the ε phase was observed to nucleate only at the surface (and not in the bulk) of α-Fe crystallites. In such an OR, the smallest angle between $(203)_\varepsilon$ and $(001)_\alpha$ planes is about 30° that is obviously not the case in our samples. This fact supports the assumption that in our samples the ε phase is formed from α-Fe via the γ' phase.

Thus, at the conditions applied the $\gamma' \rightarrow \varepsilon$ transformation of the Fe-sublattice can also be described in terms of a martensitic transition. The OR formed is defined by

$$[010]_\varepsilon || [1\bar{1}0]_{\gamma'}, \tag{21}$$

$$(001)_\varepsilon || (111)_{\gamma'} \tag{22}$$

and features parallelity of c.p.d.'s and c.p.p.'s between the precipitates and the parent matrix.

To complete the discussion on phase transformations in the Fe-N system, we will address the morphology of the samples. As was observed in our previous experiments,[48] thin epitaxial Fe layers deposited onto MgO(001) exhibit a high degree of crystallinity and an atomically flat interface with the metallic cap layer. The elastic strain caused by the lattice mismatch with the substrate was found to be fully relaxed for Fe film thicknesses exceeding 200 Å. Formation of the bct α', α'' phases in the films results in elastic distortion of the bcc lattice in the direction perpendicular to the sample surface. In the case of films with the (001) surface orientation, formation of the bct phase with OR as defined by Eqs. (5) and (6) will probably lead to a layer that is homogeneously (anisotropically) expanded in the direction normal to the surface. In epitaxial systems, the presence of substrate can cause additional energetic barriers for phase transformations. In the case considered, the as-deposited epitaxial Fe layer is fully relaxed meaning that no (or very little) stress is imposed. Since the lattice parameter of α'-Fe_8N and α''-$Fe_{16}N_2$ is about the same as of α-Fe along the layer-substrate interface, the influence of the substrate on the transformation would be minor. In accordance with the transformation model described above, the $\alpha' \rightarrow \gamma'$ phase transition gives rise to the formation of fcc γ' crystallites, which OR with respect to the parent α' matrix is defined by Eqs. (15) and (16). Upon further transformation, the fcc γ' crystallites break up into hcp ε crystallites with an OR as in Eqs. (21) and (22). Thus, an overall $\alpha \rightarrow \alpha'$, $\alpha'' \rightarrow \gamma' \rightarrow \varepsilon$ phase transformation process in the Fe-N system is accompanied by a grain refinement. The described $\alpha' \rightarrow \gamma'$ as well as the $\gamma' \rightarrow \varepsilon$ transformations are likely to result in lamella-type of macrostructure. With such morphology strong adhesion of the layers to the substrate is improbable. In our experiments we observed that ultrasonic treatment of the γ'-Fe_4N and ε-Fe_xN samples makes the layers peel off the substrate. This is in agreement with the morphology predicted.

IV. CONCLUSIONS

Summarizing, phase transformations during low-temperature gaseous nitriding in epitaxial Ni-capped Fe layers were studied. It was shown that upon low-temperature gaseous nitriding of Ni/Fe bilayers, virtually any Fe nitride can be produced as a pore-free material. Only the ζ phase was not clearly observed in our samples. We cannot exclude the fact that a small fraction of ζ-Fe_2N was present together with the high-N-content ε-Fe_xN phase. The CEMS spectra of these two phases are very similar.[49,28] The positions of the (101), (102), and (203) XRD peaks observed in our experiments for (textured) ε could be very close to those of (211), (212), and (423) of ζ and, if the amount of the ζ phase in the samples was small, the peaks could be missed.

It was found that a higher nitriding potential value was needed to produce a certain Fe-N phase in the epitaxial Ni/Fe bilayers, compared to the value given by the Lehrer diagram measured for polycrystalline material. The delay was explained by a lack of nucleation sites (such as lattice defects) in the epitaxial Fe layers.

Our studies showed that at relatively low temperatures where diffusion of Fe atoms can be neglected, phase transformations in the Fe-N system can be well described in terms of martensitic transitions, as far as the Fe sublattice is concerned. During gaseous nitriding of α-Fe in the 200 °C –300 °C temperature range, the phase transformations occur in the bcc→bct→fcc→hcp sequence. It was confirmed that, if formed in a thin film, the γ' precipitates have the orientation relationship with the nitrogen martensite matrix α' as defined by Eqs. (17) and (18). This orientation relationship is achieved by simultaneous half twin shear in the $(1\bar{1}2)_{\alpha'}$ plane along the $[1\bar{1}1]_{\alpha'}$ direction, and a distortion along the principal crystallographic axes. It is inevitable that shear is accompanied by slip or twinning. We did not investigate this

point. Possibly this twinning could induce a lamellae type of morphology in the sample.[39,50,51] It was also shown that the orientation of the ε precipitates with respect to the host matrix of γ' is as described by Eqs. (21) and (22). This relationship is probably due to simultaneous shear of every other $(111)_{\gamma'}$ plane along the $[11\bar{2}]_{\gamma'}$ direction and a distortion along the principal axes.

Finally, it was demonstrated that each step of the $\alpha \rightarrow \alpha' \rightarrow \gamma' \rightarrow \varepsilon$ transformation cycle is accompanied by grain refinement.

*Author to whom correspondence should be addressed. Present address: Philips Research Laboratories, Storage Physics (WY31), Prof. Holstlaan 4, 5656 AA Eindhoven, The Netherlands. FAX: 31 40 2744648, Email address: andrei.mijiritskii@philips.com

[1] K. H. Jack, Proc. R. Soc. London, Ser. A **208**, 200 (1951).
[2] R. C. Ruhl and M. Cohen, Trans. Metall. Soc. AIME **245**, 241 (1969).
[3] H. Nakagawa, S. Nasu, H. Fujii, M. Takahashi, and F. Kanamaru, Hyperfine Interact. **69**, 455 (1991).
[4] P. Schaaf, C. Illgner, M. Niederdrenk, and K. P. Lieb, Hyperfine Interact. **95**, 199 (1995).
[5] L. Rissanen, P. Schaaf, M. Neubauer, K.-P. Lieb, J. Keinonen, and T. Sajavaara, Appl. Surf. Sci. **138-139**, 261 (1999).
[6] G. Marest, Defect Diffus. Forum **57/58**, 273 (1988).
[7] M. Kumoro, Y. Kozono, M. Hanazono, and Y. Sugita, J. Appl. Phys. **67**, 5126 (1990).
[8] E. H. du Marchie van Voorthuysen, B. Feddes, N. G. Chechenin, D. K. Inia, A. M. Vredenberg, and D. O. Boerma, Phys. Status Solidi A **177**, 127 (2000).
[9] D. K. Inia, W. M. Arnoldbik, A. M. Vredenberg, and D. O. Boerma, Surf. Eng. **12**, 326 (1996).
[10] D. K. Inia, M. H. Pröpper, W. A. Arnoldbik, A. M. Vredenberg, and D. O. Boerma, Appl. Phys. Lett. **70**, 1245 (1997).
[11] A. Ozaki and K. I. Aika, in *A Treatise on Dinitrogen Fixation*, edited by R. W. F. Hardy, F. Bottomley, and R. C. Burny (Wiley, New York, 1979), Chap. 4, p. 169.
[12] G. Ertl, M. Huber, and N. Thiele, Z. Naturforsch. A **34**, 30 (1979).
[13] Y. Cohen and I. Riess, Mater. Sci. Eng., B **15**, 160 (1992).
[14] A. V. Mijiritskii, P. J. M. Smulders, V. Ya. Chumanov, O. C. Rogojanu, M. A. James, and D. O. Boerma, Phys. Rev. B **58**, 8960 (1998).
[15] E. Lehrer, Zeitschrift Elektrochemie. **36**, 383 (1930).
[16] B. J. Kooi, M. A. J. Somers, and E. J. Mittemeijer, Metall. Mater. Trans. A **27**, 1063 (1996).
[17] K. H. Jack, Proc. R. Soc. London, Ser. A **208**, 216 (1951).
[18] S. Okamoto, O. Osami, and Y. Shimada, J. Magn. Magn. Mater. **208**, 102 (2000).
[19] L. de Wit and F. W. Saris, Mater. Sci. Eng., A **199**, 219 (1995).
[20] H. C. F. Rozendaal, E. J. Mittemeijer, P. F. Colijn, and P. J. van der Schaaf, Metall. Trans. A **14**, 395 (1983).
[21] Y. Iijima, J. Alloys Compd. **234**, 290 (1996).
[22] D. M. Borsa and S. Yu. Grachev (private communication).
[23] A. M. Vredenberg, C. M. Pérez-Martin, J. S. Custer, D. O. Boerma, L. de Wit, F. W. Saris, N. M. van der Pers, T. H. de Keijser, and E. J. Mittemeijer, Surf. Coat. Technol. **51**, 79 (1992).
[24] L. de Wit, T. Weber, J. S. Custer, and F. W. Saris, Phys. Rev. Lett. **72**, 3835 (1994).
[25] D. K. Inia, A. M. Vredenberg, and D. O. Boerma, F. D. Tichelaar, H. Schut, and A. van Veen, J. Mater. Res. **14**, 2674 (1999).
[26] M. Grujicic and P. Dang, Mater. Sci. Eng., A **201**, 194 (1995).
[27] B. J. Kooi, Ph.D. thesis, Technical University Delft, 1995.
[28] G. M. Chen, N. K. Jaggi, J. B. Butt, E. B. Yeh, and L. H. Schwartz, J. Phys. Chem. **87**, 5326 (1983).
[29] K. H. Jack, Acta Crystallogr. **5**, 404 (1952).
[30] A. Oueldennaoua, E. Bauer-Grosse, M. Foos, and C. Frants, Scr. Metall. **19**, 1503 (1985).
[31] K. Suzuki, H. Morita, T. Kaneko, H. Yoshida, and H. Fujimori, J. Alloys Compd. **201**, 11 (1993).
[32] L. Rissanen, M. Neubauer, K.-P. Lieb, and P. Schaaf, J. Alloys Compd. **274**, 74 (1998).
[33] Y. Kong, J. Phys.: Condens. Matter **12**, 4161 (2000).
[34] L. S. Darken, *The Physical Chemistry of Metallic Solutions and Intermetallic Compounds* (H. M. S. O., London, 1959).
[35] R. C. Weast, *Handbook on Chemistry and Physics*, 57th ed. (CRC Press, Cleveland, 1977).
[36] D. A. Porter and K. E. Easterling, *Phase Transformations in Metals and Alloys* (Van Nostrand Reinhold, New York, 1981).
[37] A. H. Cottrell, *An Introduction to Metallurgy* (Edward Arnold, London, 1967).
[38] H. A. Wriedt, N. A. Gokcen, and R. H. Nafziger, Bull. Alloy Phase Diagrams **8**, 355 (1987).
[39] T. Lyman, *Metals Handbook: Metallography, Structures and Phase Diagrams* (Am. Soc. Metals, Metals Park, Ohio, 1973), Vol. 8.
[40] W. Pitsch, Arch. Eisenhuettenwes. **32**, 493 (1961).
[41] W. Pitsch, Arch. Eisenhuettenwes. **32**, 573 (1961).
[42] W. Pitsch, Philos. Mag. **4**, 577 (1959).
[43] P. Haasen, *Physical Metallugry* (Cambridge University Press, Cambridge, 1978).
[44] U. Dahmen, Metallurgica **30**, 63 (1982).
[45] Y. Inokuti, N. Nishida, and N. Ohashi, Metall. Trans. A **6**, 773 (1975).
[46] G. R. Booker, J. Norbury, and A. L. Sutton, J. Iron Steel Inst., London **187**, 205 (1957).
[47] P. G. Shewmon, *Transformations in Metals* (McGraw-Hill, New York, 1969).
[48] A. V. Mijiritskii and D. O. Boerma J. Magn. Magn. Mater. **232/1-2**, 105 (2001).
[49] J. Bainbridge, D. A. Channing, W. H. Willow, and R. E. Pendleburg, J. Phys. Chem. Solids **34**, 1579 (1973).
[50] R. Priestner and W. C. Leslie, Philos. Mag. **11**, 895 (1965).
[51] J. Th. M. De Hosson, in *Intermetallic and Ceramic Coatings*, edited by N. B. Dahorte and T. S. Sudarshan (Marcel Dekker, New York, 1999).